scientific reports

Check for updates

OPEN

Human heart-on-a-chip microphysiological system comprising endothelial cells, fibroblasts, and iPSC-derived cardiomyocytes

Yun Liu, Rumaisa Kamran, Xiaoxia Han, Mengxue Wang, Qiang Li, Daoyue Lai, Keiji Naruse & Ken Takahashi✉

In recent years, research on organ-on-a-chip technology has been flourishing, particularly for drug screening and disease model development. Fibroblasts and vascular endothelial cells engage in crosstalk through paracrine signaling and direct cell–cell contact, which is essential for the normal development and function of the heart. Therefore, to faithfully recapitulate cardiac function, it is imperative to incorporate fibroblasts and vascular endothelial cells into a heart-on-a-chip model. Here, we report the development of a human heart-on-a-chip composed of induced pluripotent stem cell (iPSC)-derived cardiomyocytes, fibroblasts, and vascular endothelial cells. Vascular endothelial cells cultured on microfluidic channels responded to the flow of culture medium mimicking blood flow by orienting themselves parallel to the flow direction, akin to in vivo vascular alignment in response to blood flow. Furthermore, the flow of culture medium promoted integrity among vascular endothelial cells, as evidenced by CD31 staining and lower apparent permeability. The tri-culture condition of iPSC-derived cardiomyocytes, fibroblasts, and vascular endothelial cells resulted in higher expression of the ventricular cardiomyocyte marker IRX4 and increased contractility compared to the bi-culture condition with iPSC-derived cardiomyocytes and fibroblasts alone. Such tri-culture-derived cardiac tissues exhibited cardiac responses similar to in vivo hearts, including an increase in heart rate upon noradrenaline administration. In summary, we have achieved the development of a heart-on-a-chip composed of cardiomyocytes, fibroblasts, and vascular endothelial cells that mimics in vivo cardiac behavior.

Keywords Induced pluripotent stem cells, Fibroblasts, Endothelial cells, Heart, Heart-on-a-chip, Organ-on-a-chip

Cardiovascular disease poses a significant threat to human health[1], making the creation of disease models related to cardiovascular issues an imperative task. While animal models, such as mice, have traditionally played a pivotal role in this field due to their ease of reproduction and genetic manipulability, their use in cardiovascular research is fraught with two significant inherent problems: inaccuracies in extrapolating data from animals due to differences in cardiac physiology[2,3], and ethical concerns surrounding animal use. An alternative approach to disease modelling is through cell culture. Typically, cell culture models differ from structure of human tissues. Moreover, conventional culture methods struggle to replicate the microenvironment and intercellular communication, including direct contact, paracrine signaling, and extracellular vesicle interactions, which are essential for cellular growth and development[4,5].

Currently, significant advancements, such as the implementation of perfusion and mechanical or electrical stimulation in bioreactors, have been achieved in cardiac tissue engineering[6,7]. Nevertheless, traditional static culture models remain indispensable long-term tools for cardiac drug screening[8]. The field of cardiac tissue engineering has made strides in constructing miniature cardiac tissues in vitro, and the integration of microfluidic

Department of Cardiovascular Physiology, Graduate School of Medicine, Dentistry and Pharmaceutical Sciences, Okayama University, Okayama City 700-8558, Japan. ✉email: takah-k2@okayama-u.ac.jp

technology has further accelerated its development[9,10], leading to enhanced prediction of drug responses in the human body.

Various approaches are employed in cardiac tissue engineering, including cell-sheet engineering[11,12], organoids[13], scaffold-based myocardial tissue engineering[14–16], and 3D bioprinting technology[17,18]. While scaffold-free cardiac tissue engineering and 3D bioprinting technology have their own advantages, they also come with associated limitations. For instance, scaffold-free methods fail to guarantee directional alignment of generated myocardial cells comparable to adult myocardial cells in vivo[19], while 3D bioprinting technology faces challenges in resolution and deposition speed[19]. Due to the isolating effect of scaffold systems, myocardial tissues formed using scaffold technology may still be unable to reproduce the interactions between cells and the matrix[20], although scaffolds can enhance the mechanical performance of myocardial tissue[21,22].

Additionally, scaffold systems serve as a platform for microfluidic systems, enabling an effective way for perfusion culture to simulate continuous mechanical and physical stimuli on cells during myocardial cell growth[23–25]. In recent years, research findings on microfluidic systems have been gradually emerged, with many studies mainly focusing on the application of stimulating factors in microfluidic systems to promote the differentiation of stem cells and the growth of myocardial cells[26–28]. However, some studies lack relevant results regarding the permeability of the endothelial cell layer in microfluidic systems and the impact of endothelial cells on the differentiation of induced pluripotent stem (iPS) cells[29–31].

The heart is mainly composed of cardiomyocytes, cardiac fibroblasts, and endothelial cells[32]. Cardiac function is not solely dictated by cardiomyocytes but is also influenced by the interactions between cardiac fibroblasts and endothelial cells. Specifically, cardiomyocytes are known to establish gap junctions with fibroblasts, contributing to the establishment of normal electrical excitation in the heart[33,34]. Additionally, endothelial cells and cardiomyocytes communicate through nitric oxide, fatty acids, and exosomes, which play critical roles in the normal development and postnatal function of the heart[35]. Consequently, co-culturing cardiomyocytes, fibroblasts, and endothelial cells is essential for accurately replicating heart function.

Several previous studies, including ours, have shown that co-culturing cardiomyocytes with fibroblasts leads to myocardial tissue structures and functions that more closely resemble those of the in vivo heart[36–38]. In this study, our objective is to further recapitulate the structure and function of the heart more faithfully by incorporating endothelial cells into this bi-culture system. Furthermore, we provide new value by enabling drug delivery from the vascular side and measurement of vascular permeability.

In this study, we developed a heart-on-a-chip model by pre-seeding human umbilical vein endothelial cells (HUVEC) in a microfluidic channel (Fig. 1). We investigated the effects of medium flow, which mimics blood flow in the vasculature, on endothelial cell morphology and functionality. Endothelial cells exhibited changes in orientation in response to the flow of culture medium, along with the formation of cell–cell junctions mediated by CD31, leading to an enhancement of barrier function. Additionally, by seeding iPSCs and human gingival

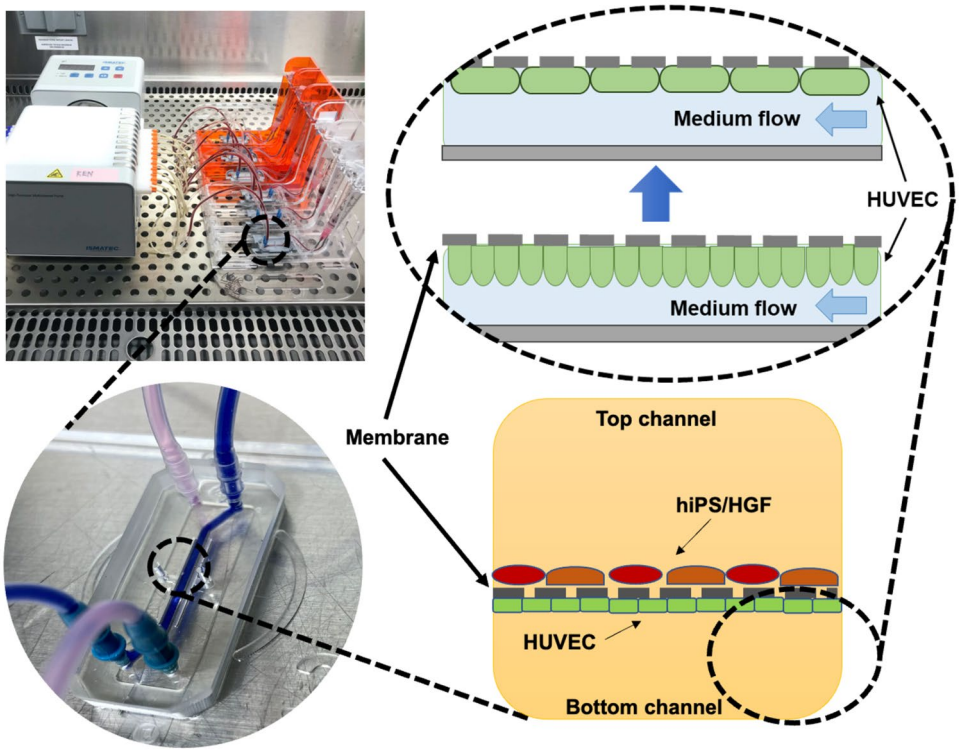

Figure 1. Perfusion system for the heart-on-a-chip. Endothelial cells are seeded in the bottom channel of the microfluidic chip, while induced pluripotent stem cells and fibroblasts are seeded in the top channel. The culture medium is delivered by a peristaltic pump.

fibroblasts (HGF) in another microfluidic channel adjacent to the endothelial channel, iPSC-derived cardiomyocytes exhibited increased expression of the ventricular cardiomyocyte marker IRX4 and stronger contractility, compared to iPSC-CM-fibroblast bi-culture. The tri-culture heart-on-a-chip exhibited sensitivity to noradrenaline (NA) and nifedipine similar to that of adult cardiomyocytes. In summary, we developed an iPSC-CM-fibroblast-endothelial tri-culture heart-on-a-chip that better recapitulates heart development and function.

Results

Impact of fluid flow on cell alignment

We employed microfluidic chips equipped with two microchannels, namely, top and bottom channels, to create a heart-on-a-chip model. Initially, HUVECs were seeded in the bottom channel of the microfluidic chip. After continuous perfusion of HUVECs for 4 days, the lower 'vascular' channel membrane was entirely covered by HUVECs. These HUVECs responded to fluid shear stress by aligning themselves parallel to the direction of medium flow. Under the 'no flow' condition, the cells did not exhibit any directional preference (Fig. 2a and b). In contrast, under the 'flow' condition, the cells displayed an elongated, spindle shape with a clear directional preference (Fig. 2c and d). The results of the directional analysis showed that under the 'no flow' condition, HUVECs lacked a specific orientation. However, under the 'flow' condition, a distinct directional preference with a peak at 0° was observed. Specifically, the frequency of cell directionality within the range of −20° to 20° was 27.3 ± 3.3% (n = 6) under the 'no flow' condition, while it reached 38.6 ± 7.8% (n = 5) under the 'flow' condition. ($P < 0.01$) (Fig. 2e).

Furthermore, we conducted a directional analysis of cells by varying the flow rates from 0 to 160 µl/h (Fig. 2f). As a result, the directional preference toward the direction of fluid flow (0°) became evident at flow rates of 40 µl/h or higher, with a pronounced effect observed at 80 µl/h or above. Additionally, the flow of the medium also had a significant impact on the orientation of F-actin within endothelial cells (Fig. 2g). The orientation of F-actin was unclear under the 'no flow' condition, while a clear alignment towards the direction of flow was observed under the 'flow' condition. Based on these results, a flow rate of 80 µl/h was employed for perfusion hereafter.

Impact of fluid flow on the integrity of endothelial cell

Next, we evaluated the endothelial layer's barrier function by immunostaining specific marker of endothelial cells and quantifying apparent permeability. Immunostaining for the CD31 protein was conducted (Fig. 3a), revealing an orientation toward the flow direction of endothelial cells similar to that observed in Fig. 2a. Additionally, while CD31 immunofluorescence staining indicated the integrity of endothelial layer presence in both groups, the 'flow' condition exhibited a significantly higher average fluorescence intensity compared to the 'no-flow' condition (127.1 ± 4.8 and 110.2 ± 5.6, respectively, n = 11 for each) ($P < 0.05$) (Fig. 3b).

Furthermore, we determined the apparent permeability from the bottom 'vascular' channels to the top 'cardiac' channels using Texas Red-conjugated dextran (MW: 3000). Between day 5 and day 7 post-seeding of HUVECs, the cells in the flow condition consistently showed a reduction in permeability, decreasing from $1.57 \times 10^{-5} \pm 3.17 \times 10^{-5}$ cm/s (n = 8, day 5) to $8.32 \times 10^{-6} \pm 1.07 \times 10^{-5}$ cm/s (n = 10, day 7), representing a 47% reduction. This reduction suggests an enhancement in endothelial barrier function. In contrast, cells in the 'no flow' condition exhibited relatively higher permeability of $5.20 \times 10^{-5} \pm 4.29 \times 10^{-5}$ cm/s (n = 8, day 7) ($P < 0.05$) (Fig. 3c). Vascular permeability is closely related to the pathophysiology of atherosclerosis and is crucial for the manifestation of normal vascular function. The presence of the endothelial cell layer can enhance the differentiation of iPS cells and functionality of myocardial cells[39,40]. Based on the results above, a combination of 10,000 iPSCs and 1,700 HGFs was applied onto the top channels. Subsequently, the iPSC differentiation protocol was implemented over the ensuing days.

Endothelial cells enhance the contractility of iPS-CMs

The cardiac tissue exhibited spontaneous contraction, with iPS-CMs maintaining this activity throughout the experimental period, which extended to ~ 60th day in this study (Supplementary Video 1). We compared the contractility of iPS-CMs co-cultured with HUVECs (tri-culture group) to those without HUVECs (bi-culture group). We recorded videos of beating CMs in both groups on Day 22 (n = 4 biological replicates for each group). From the analysis of 8 recordings (tri-culture group: n = 4, bi-culture group: n = 4), we observed that the average contractility of iPS-CMs in the tri-culture group was 5.45 ± 1.09, which was significantly higher than that of iPS-CMs in the bi-culture group (2.65 ± 0.52) ($P < 0.01$) (Fig. 4a and b).

Endothelial cells promote cardiac marker expression in iPS-CMs

To investigate whether the high contractility in the tri-culture group is supported by the expression of cardiomyocyte markers, flow cytometry analysis of cardiomyocyte marker expression was performed. In the negative control (HUVEC monoculture), the expression rate of the cardiomyocyte marker cardiac troponin t (cTnT) was 0.1%, whereas it reached 64.8% in a bi-culture sample and 92.8% in a tri-culture sample (Fig. 5a). Although the difference of cTnT expression did not reach statistical significance between two groups, it showed a trend of being higher in the tri-culture group (64.6 ± 22.9%, n = 5) as opposed to the bi-culture group (55.9 ± 6.6%, n = 6) (Fig. 5b).

Following that, we conducted an expression analysis of the ventricular cardiomyocyte marker IRX4. The tri-culture group exhibited significantly higher IRX4 expression compared to the bi-culture group ($P < 0.05$, as shown in Fig. 5c). Additionally, the percentage of cells co-expressing cTnT and IRX4 was notably elevated in the tri-culture group (56.3 ± 14.7%, n = 5) in contrast to the bi-culture group (30.2 ± 13.5%, n = 6) ($P < 0.05$) (depicted in Fig. 5d and e).

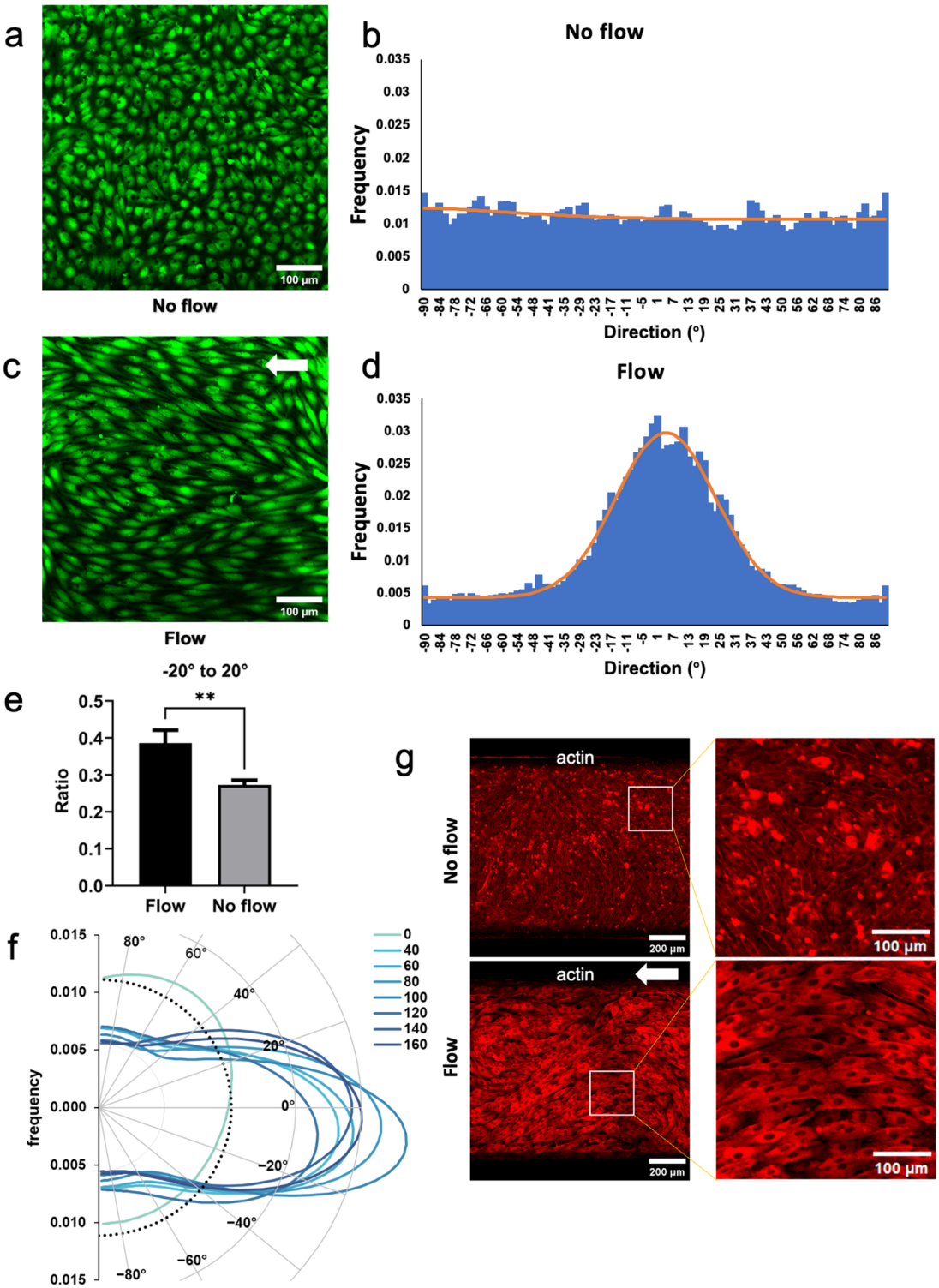

Figure 2. Response of vascular endothelial cells to medium flow. Vascular endothelial cell response to medium flow was examined by seeding HUVECs in microfluidic channels without (**a**) and with (**c**) medium flow to study their reaction to fluid shear stress. HUVECs from the same source were divided into the control and flow groups, with the experiments conducted simultaneously. Only HUVECs with passage numbers between 3 to 8 were used in this study, and calcium-sensitive dye Cal-520 was employed to visualize the cell layer. Frequency histograms of directionality in both groups are depicted in (**b**) and (**d**). If there is no orientation in the cell images, the frequency in each bin becomes 0.011. The 0° position signifies the direction of fluid flow in the culture medium. A comparison of total frequencies in the range from − 20° to + 20° is shown in (**e**). $^{**}P < 0.01$. (**f**) Polar representation of directional analysis under varying flow rates of the culture medium is illustrated, with dotted lines indicating a frequency of 0.011 when there is no orientation in the images. (**g**) displays a staining image of F-actin in vascular endothelial cells.

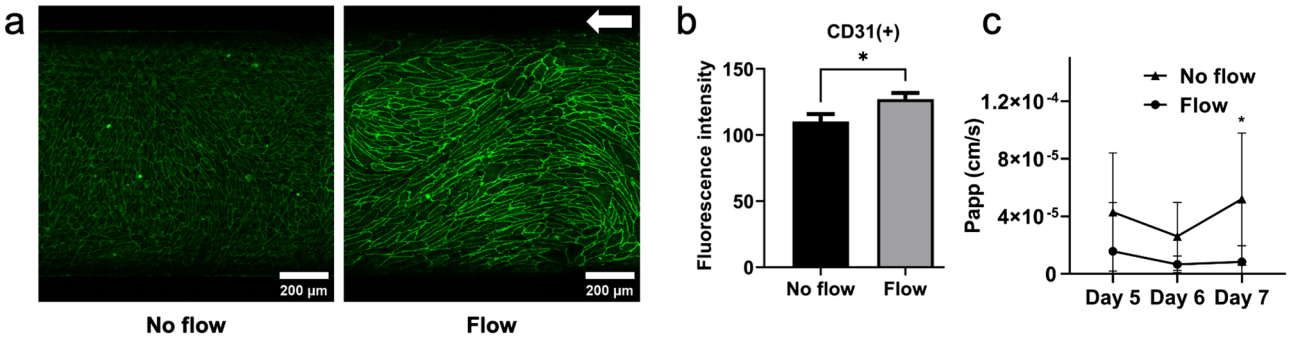

Figure 3. Barrier Function of Vascular Endothelial Cells. (**a**) Comparison of fluorescent immunostaining image of cell–cell junction protein CD31 under flow and no-flow conditions. (**b**) Comparison of fluorescence intensity in CD31 staining. (**c**) Analysis of the apparent permeability (P_{app}) of the vascular endothelial cell layer over time. *P < 0.05.

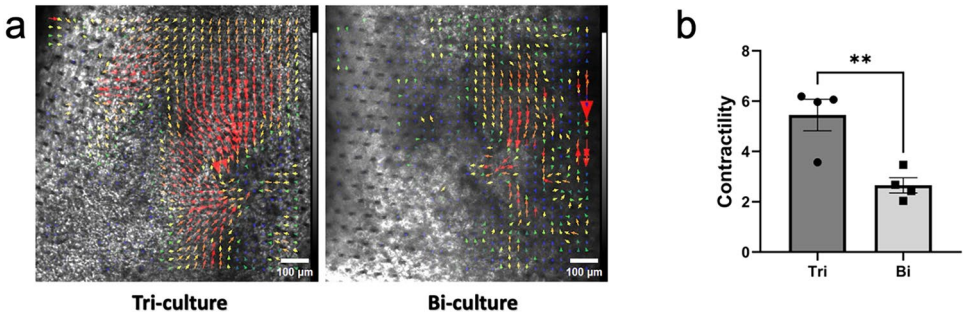

Figure 4. Analysis of cardiac tissue contractility. (**a**) Comparison of the vector field of cardiac contractility between tri-culture and bi-culture conditions. Longer vectors indicate higher contractility at the respective sites. (**b**) Comparison of the sum of cardiac contractility between tri-culture and bi-culture conditions. *P < 0.05.

Triculture of iPS-CMs, fibroblasts, and endothelial cells in the microfluidic system produces three dimensional myocardial tissue

Following the establishment of a low permeability layer by HUVECs in the vascular channel, iPSCs and fibroblasts were seeded in the adjacent cardiac channel. Typically, approximately two weeks after initiating the differentiation protocol, myocardial tissue comprising iPS-CMs and fibroblasts forms a multilayered structure (Fig. 6a–c). Multilayered cells were observed in z-stack confocal microscopy images of myocardial tissue, approximately 530 μm thick, with nuclei stained using Hoechst 33342 (Fig. 6b). Hematoxylin–eosin staining images of paraffin sections confirmed the formation of a layer approximately 840 μm thick at its thickest point (Fig. 6d). The cardiomyocytes exhibit a high degree of alignment in the direction of the flow path (Fig. 6e). Immunostaining of cTnT in paraffin sections reveals highly oriented and distinct sarcomere structures (Fig. 6f).

Response of iPS-CMs to NA

One of the crucial features of cardiomyocytes is their responsiveness to neurohormonal stimulation, such as that induced by NA[41]. The cardiac tissue in this study demonstrated a dose-dependent positive chronotropic effect in response to NA.

To observe the physiological response of cardiac channel tissues, we administered NA, a β-adrenergic agonist (Fig. 7a–c), to tri-culture hiPS-CMs tissues. We observed that NA increased the heart rate of iPSC-CMs in a dose-dependent manner (Fig. 7b). The dose–response relationship of NA was fitted with a sigmoid curve allowing a variable slope, resulting in a Hill coefficient of 0.56 and an EC50 of 24.8 μM (95% confidence interval: 0.73–83.88 μM, n = 4). When the NA concentration was elevated to 1 mM, it resulted in a heart rate of 139.5 ± 10.4, which was 2.61 times the baseline. While NA slightly increased the contractility of cardiac tissue, this effect was modest compared to the increase in heart rate (Fig. 7c).

Response of iPS-CMs to nifedipine

Subsequently, we administered nifedipine, a $Ca_v1.2$ channel inhibitor, to cardiac channel tissue (Fig. 7d–f). Nifedipine, ranging from 0 nM to 1000 nM, was perfused to the tri-culture hiPS-CMs tissues. It did not significantly impact heart rate; however, it elicited a dose-dependent and notably significant decrease in contractility.

Moreover, we examined intracellular calcium ion dynamics in cardiac tissue using the calcium-sensitive dye Cal-520 (Supplementary Video 2). iPS-CMs displayed a periodic, coordinated pattern of calcium influx

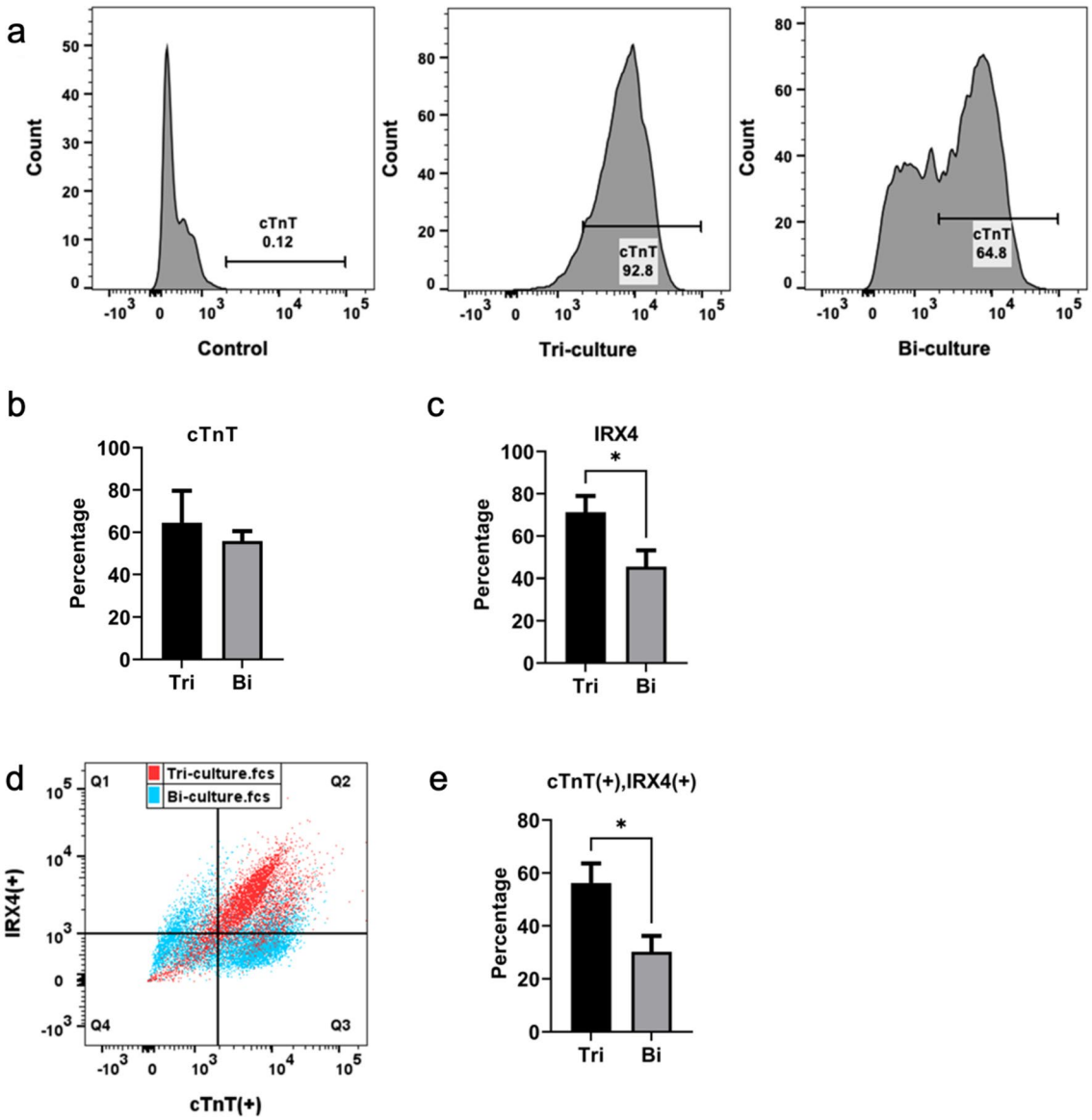

Figure. 5. Expression analysis of cardiac marker proteins. (**a**) Flow cytometry analysis of cTnT expression in cardiac marker proteins. Control: non-differentiated iPSCs. (**b**) Comparison of cTnT expression levels between the tri-culture and bi-culture groups. (**c**) Comparison of the expression levels of ventricular cardiomyocyte marker IRX4 in the tri-culture and bi-culture groups. (**d**) Analysis of cTnT and IRX4 expression levels by flow cytometry. Red: tri-culture, Blue: bi-culture. (**e**) Comparison of the number of cells co-expressing cTnT and IRX4 between the tri-culture and bi-culture groups. *P < 0.05.

synchronized with their contraction under a fluorescence microscope (Fig. 7g and h). Fluorescence imaging of calcium transients revealed a consistent pattern of intracellular fluorescence level changes correlated with myocardial contraction. Specifically, fluorescence intensity increased during systole, followed by a decrease during diastole, ultimately returning to baseline. The interval between transient peaks remained consistent throughout the measurement duration (approximately 30 s), with no observed arrhythmias.

Upon normalizing the peak height of the calcium transient, the time to peak decreased in a dose-dependent manner with nifedipine (Fig. 7i and j). In contrast, CaTD90, representing the calcium transient duration at 90% recovery, increased in a dose-dependent manner (Fig. 7i and k).

Discussion

Presently, tissue engineering strategies involve 3D reconstruction and incorporate organoids or micro-bioreactors as complementary elements to conventional cell culture models. Moreover, utilizing iPSCs for CM differentiation not only addresses ethical concerns linked to animal models but also facilitates the sourcing of cells from both healthy donors and patients with specific conditions, allowing for a more faithful reproduction of the original donor's genotype[42,43]. Additionally, 3D culture models more accurately mimic the normal physiological and anatomical structures of the human body[44], rendering them more representative of organ system physiology.

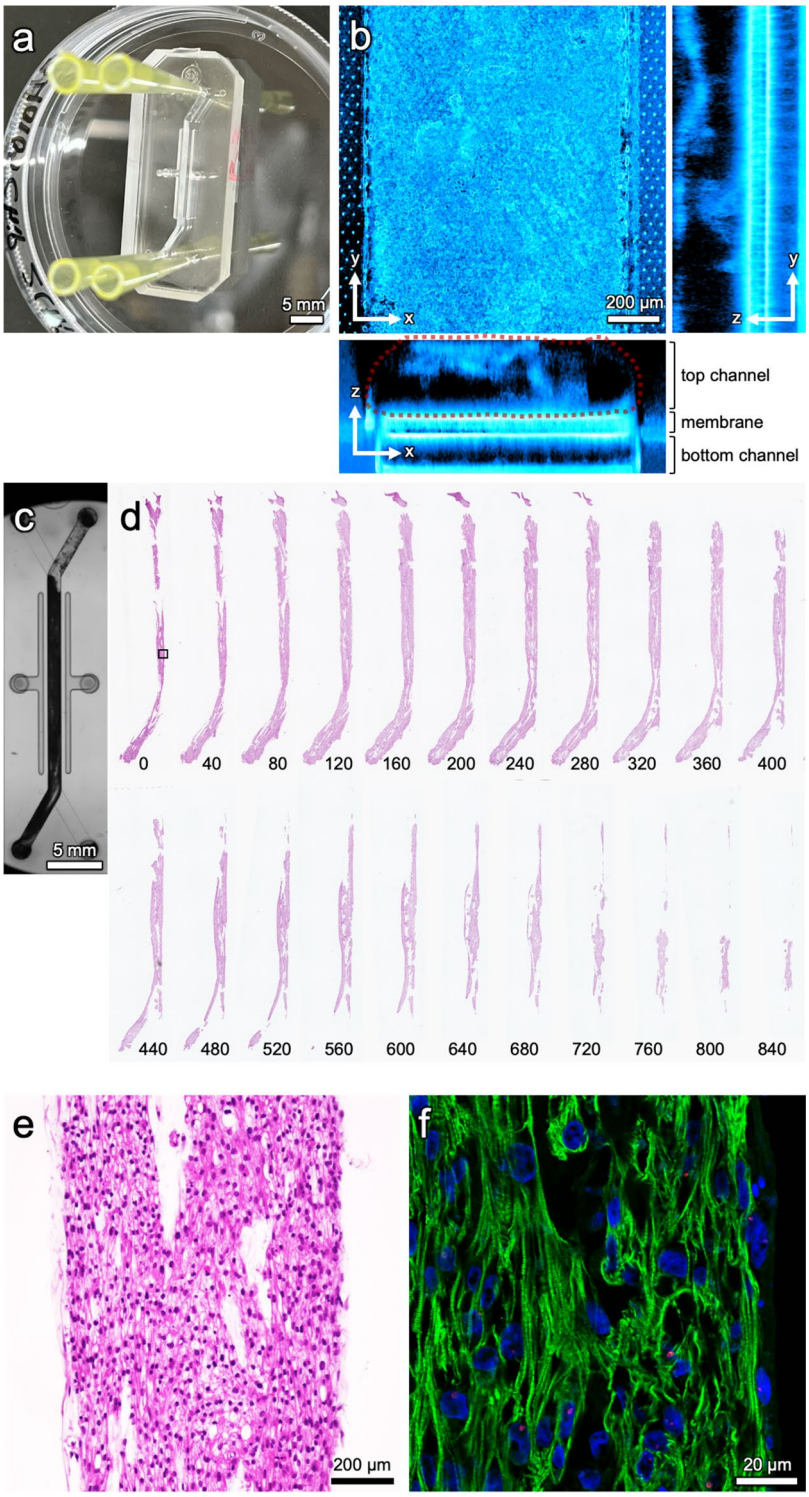

Figure. 6. 3D structure of cardiac tissue in a tri-culture heart-on-a-chip. (**a**) Microfluidic chip with the perfusion tube removed. White tissue can be observed in the top channel macroscopically. (**b**) Cross-sectional z-stack images of cells in a microfluidic chip, captured in the xy, yz, and xz planes using a confocal microscope. DAPI staining highlights cells, and in the yz and xz plane images, cells are seen adhering to both the top channel side and bottom channel side, separated by a 50 µm thick membrane. The cell tissue on the top channel side measures approximately 230 µm in thickness, with only the surface of the thick tissue stained with DAPI. Red dashed lines in the xz plane indicate clusters of cells in the top channel. (**c**) In the microfluidic channel, a dark, high-density cluster of cells is visible in the transmitted light microscopy image. (**d**) The paraffin-embedded serial sections of cardiac tissue in the top channel are depicted in the hematoxylin–eosin (H–E) staining image. Distances (µm) from the lowest plane are indicated by numbers. The square in the 0 µm plane designates the location of the magnified image in (**e**). (**e**) The H-E staining image of cardiac tissue reveals densely packed cytoplasm oriented in the direction of the vertical microfluidic channel. (**f**) Immunocytochemistry images of heart-on-chip tissue which showed the cTnT location.

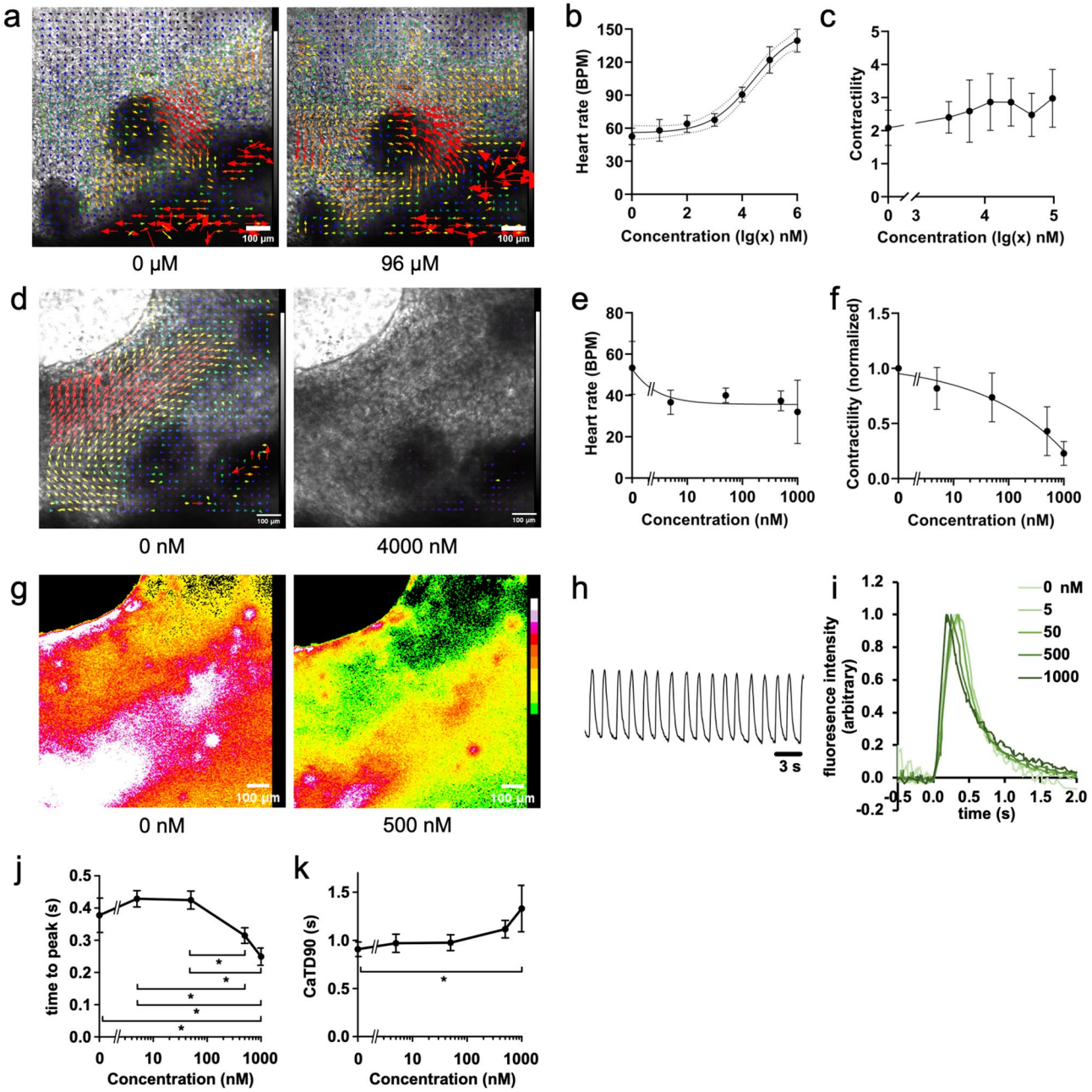

Figure. 7. Response of cardiac tissue to NA and nifedipine. (**a**) Vector field analysis of cardiac tissue contractility before and after NA administration. (**b**) Dose–response curve of NA on heart rate. Estimated EC_{50} is 24.8 μM based on sigmoid curve fitting. (**c**) Dose–response curve of NA on contractility. (**d**) Vector field analysis of cardiac tissue contractility before and after nifedipine administration. (**e**) Dose–response curve of nifedipine on heart rate. (**f**) Dose–response curve of nifedipine on contractility. (**g**) Intracellular calcium ion levels in cardiac tissue before and after nifedipine administration. (**h**) Calcium transient (CaT) trace of cardiac tissue without nifedipine administration. (**i**) Overlay of CaT curves for nifedipine administration at 0, 5, 50, 500, and 1000 nM. Fluorescence intensity is normalized at the level of peak values. **j**. Dose–response curve of nifedipine for time to peak in CaT curves. (**k**) Dose–response curve of nifedipine for CaT duration at 90% recovery (CaTD90). *$P < 0.05$.

In this study, we have developed a 3D heart-on-a-chip model using iPSCs, fibroblasts, and endothelial cells, designed to mimic the anatomical structure of cardiac tissue. As demonstrated in previous studies, including our own[37,45], co-culture with fibroblasts enhances the contractile function of the heart. The addition of vascular endothelial cells to these bi-culture systems in this study holds significant importance, as it brings the heart model even closer to the structure and function of the in vivo heart. There is prior research on heart chips using microfluidic channels, including co-culture systems of iPS cardiomyocytes and vascular endothelial cells[30]. However,

our heart-on-a-chip features a stacked arrangement of myocardial tissue and vascular endothelial cell layers, offering a significant advantage in being able to measure vascular permeability.

In our bodies, vascular endothelial cells are constantly exposed to blood shear stress, initiating intracellular signaling pathways that induce changes in cellular behaviors and functions closely associated with endothelial cell functionality[46]. We applied shear stress to endothelial cells through perfusion using a peristaltic pump. Under shear stress stimulation, endothelial cells aligned parallel to the direction of the flow. The orientation of these endothelial cells is known to occur through the remodeling of F-actin, which constitutes stress fibers[47]. In this study, a clear orientation of flow-induced F-actin was observed, as expected.

Vascular permeability is closely related to the pathophysiology of atherosclerosis and is crucial for the manifestation of normal vascular function. At the branching points of blood vessels with a high incidence of atherosclerotic plaque formation, it is known that the permeability of large molecules such as low-density lipoprotein is elevated[47]. In this study, a decrease in apparent permeability was observed under shear stress induced by perfusion of the culture medium. The reduction in vascular permeability is believed to be, in part, attributed to the increased expression of CD31. It is well-documented that shear stress induced by flow upregulates the expression of CD31[48,49], a cell–cell junction protein in vascular endothelial cells, and this was observed as an increase in immunostaining intensity in this study. This suggests that the heart-on-a-chip model developed in this study faithfully recapitulates in vivo vascular function.

Cardiomyocytes derived from iPSCs often lack stable spontaneous contractions in monoculture conditions[50]. However, in contrast, the cardiac tissue generated through tri-culture in this study demonstrated stable spontaneous contractions. Additionally, co-culturing with endothelial cells led to increased contractility in iPS-CMs. This heightened contractility coincided with an upregulation in the expression of the ventricular cardiomyocyte marker protein IRX4. Hence, it is suggested that the improved contractility of iPS-CMs through co-culture with vascular endothelial cells likely results from the promotion of differentiation from iPSCs to ventricular cardiomyocytes.

One of the crucial features of cardiomyocytes is their responsiveness to neurohormonal stimulation, such as that induced by NA[41]. The cardiac tissue in this study demonstrated a dose-dependent positive chronotropic effect in response to NA. Additionally, another characteristic of cardiomyocytes is a reduction in contractility with the inhibition of calcium channels. In the human heart, inhibiting dihydropyridine calcium channels is known to weaken the contractility of ventricular muscle[51,52]. Consistently, in this study, the administration of nifedipine, a dihydropyridine calcium channel blocker, led to a reduction in the contractility of cardiac tissue. These findings suggest that the cardiac tissue in this study closely mirrors the functionality of the human heart.

Furthermore, a more detailed analysis of calcium dynamics revealed changes in the calcium transient waveform following nifedipine administration. Specifically, the time from the onset to the peak of the calcium transient was shortened in a nifedipine concentration-dependent manner, while CaTD90 was prolonged. The duration of the calcium transient correlates with the duration of the action potential, and these are associated with the QT interval on an electrocardiogram[53]. Therefore, it is expected that the heart-on-a-chip developed in this study can contribute to investigating human cardiac toxicity, such as the QT-prolonging effects of drugs.

In advanced human stem cell-derived heart-on-a-chip research, several disease models are being developed. For example, in an experimental system using human stem cell-derived cardiomyocytes, a model of ischemia–reperfusion injury has been developed that exhibits fibrosis-like symptoms and contractile abnormalities in myocardial tissue when exposed to simulated ischemia–reperfusion conditions[54]. Additionally, in heart-on-a-chip models co-culturing hiPSC-CMs with cardiac fibroblasts, an arrhythmia model has been developed by disassembling gap junction formation[55]. Thus, by simulating the characteristic changes of various diseases on heart-on-a-chips, more disease models will likely be developed in the future.

Limitations and future directions

In this study, the co-culture of cardiomyocytes, fibroblasts, and vascular endothelial cells resulted in a heart-on-a-chip with thick myocardial tissue and strong spontaneous contraction. However, the heart exhibits its physiological functions through interactions with various cell types, such as immune cells and vascular smooth muscle cells. The next research direction will be to reproduce the inflammatory responses observed during pathological condition such as ischemia–reperfusion by co-culturing with immune cells.

Paracrine signalling is essential for organ development, such as cardiomyocyte differentiation via Wnt[56] and FGF[57]. We have reported that pressure and stretch stimuli simulating blood pressure in organ chips promote nitric oxide (NO) release from endothelial cells[58]. Moving forward, we will use this system to elucidate the NO-mediated paracrine interactions between endothelial cells and cardiomyocytes.

In this study, the maximum operational period of the heart-on-a-chip was set to about 60 days. Developing a system that can operate for longer periods and creating organ models using patient-specific iPS cells are important future goals. We also examined the effects of noradrenaline and nifedipine on the heart-on-a-chip. It will be necessary to test the effects of a broader range of drugs. Comparing the QT prolongation potential between the heart-on-a-chip, human clinical data, and experimental animal data would be interesting. Through this research, we aim to verify the physiological fidelity of the heart-on-a-chip.

Methods

Cell maintenance culture

The protocols for maintaining human iPSCs and HGFs are detailed in Ref.[37]. iPSCs (201B7 cells derived from dermal fibroblasts) were cultured in StemFit AK02N medium (Cat. #: RCAK02N, Ajinomoto, Japan). Experiments were conducted using iPSCs within the 3rd and 15th passages. For HGF maintenance culture, low-glucose Dulbecco's Modified Eagle Medium (Cat. #: 11885-084, ThermoFisher Scientific, MA, USA) supplemented with

10% fetal bovine serum and 1 M-HEPES Buffer Solution (Nacalai tesque, Kyoto, Japan) was employed. All experiments were conducted using HGFs from the 11th to the 20th passages. HUVECs (Cat. #: C2519A, Lonza, Basel, Switzerland) were cultured in Endothelial Cell Growth (ECG) Medium supplemented with 2% v/v fetal calf serum (Cat. #: C-22111, PromoCell, Germany). Subculturing and maintenance cultures were performed using 3×10^5 cells at 37 °C in a 5% CO_2 atmosphere. For experiments, only HUVECs within the passage numbers of 3 to 8 were utilized.

Cell culture on microfluidic chips

For microfluidic chip experiments, we utilized the Emulate Chip S1 (Chip S1, Emulate, Boston, USA), made of polydimethylsiloxane. This chip comprises a rectangular upper channel measuring 1 mm in width, 1 mm in height, and 17 mm in length, along with a rectangular lower channel measuring 1 mm in width, 0.2 mm in height, and 17 mm in length. The upper and lower channels are separated by a thin film with a thickness of 50 μm, featuring a honeycomb-like arrangement of pores with a diameter of 7 μm, spaced at 40 μm intervals.

Before cell seeding, the chip surface was coated with growth factor reduced Matrigel (Cat. #: 354,230, Corning, USA) to enhance cell adhesion. Initially, the top channel was filled with ECG medium. Subsequently, 200,000 HUVECs in 30 μl ECG medium were pipetted into the bottom channel. The chips were then flipped and incubated overnight in an incubator. The following day, the chips were flipped back and connected to perfusion tubings (Cat. #: SC0188, Ismatec, USA), inlet medium reservoirs, effluent collection containers, and a peristaltic pump (IPC-N 24, Ismatec, USA). The inlet reservoirs were filled with ECG medium. For microfluidic chip culture, Penicillin–Streptomycin Solution (Cat. #: 168-23191, Wako, Japan) and Amphotericin B (Cat. #: A2942, Sigma, USA) were added to the culture medium at a 1:100 dilution each. The perfusion rate was set to 80 μl/h unless otherwise specified.

On the 8th day, a mixture of 100,000 iPSCs and 17,000 HGFs was seeded into the top channel. Perfusion was paused overnight to facilitate cell adhesion. The next day, the culture medium in the top channel inlet reservoir was replaced with Essential 8 medium (Cat. #: A1517001, ThermoFisher, USA), and perfusion commenced. Differentiation of iPSCs into cardiomyocytes was induced using the PSC Cardiomyocyte Differentiation Kit (Cat. #: A2921201, ThermoFisher, USA). Three days after starting perfusion with Essential 8 medium, the culture medium in the top channel inlet reservoir was changed to the differentiation medium A (component of the kit), and perfusion was initiated. After 48 h, the culture medium in the top channel inlet reservoir was switched to the differentiation medium B, and perfusion was performed. Another 48 h later, the culture medium in the top channel inlet reservoir was changed to the cardiomyocyte maintenance medium, and continuous perfusion was maintained thereafter (Fig. 8).

Permeability assay

The barrier function of endothelial cells was assessed using the method outlined by Pediaditakis et al.[59]. Texas Red-conjugated dextran (MW: 3000) (Cat. #: D3329, ThermoFisher, USA) served as a fluorescent tracer. The culture medium in the inlet reservoir of the bottom channel was replaced with a medium containing 5 μg/ml dextran and perfused for 2 h. The effluent solutions collected from the top and bottom channels were used for fluorescence measurements using a plate reader (Flexstation 3, Molecular Devices, USA). Subsequently, the apparent permeability of the dextran was calculated using the formula described in Ref.[59].

Contractility analysis of cardiac tissue

The contractility analysis of cardiac tissue is detailed in a separate publication[37]. In summary, video recordings of beating cardiac tissue were captured at a rate of 20 frames per second using a phase-contrast microscope (BZ-X710, KEYENCE, Japan) at room temperature. A discrete two-dimensional vector field of displacement, with 16 pixels by 16 pixels grid, was analyzed at each frame. The maximum size of the displacement vector over frames was determined for each grid, and the sum of these maximum sizes across all grids was defined as the contractility (dimensionless quantity) of the cardiac tissue.

Calcium imaging

The calcium indicator Cal-520 (AAT Bioquest, USA) was introduced into the culture medium at a final concentration of 5 μM and perfused for 1 h, exposing the cells to the compound. Following this, fluorescence images at a wavelength of 520 nm were captured using a fluorescence microscope (ECLIPSE TE2000-U, Nikon, Japan).

Directionality analysis utilized the Cal-520 application mentioned above to enhance the visualization of endothelial cells. Power spectrum analysis was conducted by utilizing the Directionality plugin in ImageJ[60] to Fourier-transform the acquired calcium imaging images.

In the analysis of calcium dynamics in cardiac tissue, fluorescence video imaging was conducted for 30 s at an interval of 134 ms at room temperature. Subsequently, to enhance the temporal resolution of the calcium transient (CaT) waveforms, 10 CaT waveforms recorded over 30 s were overlaid (Fig. 9). Specifically, the first CaT waveform served as a template, and the second CaT waveform was superimposed to align the peak positions. Next, the second CaT waveform was shifted to minimize the difference in fluorescence intensity values at each time point relative to the first CaT waveform. Using a similar approach, overlaying 10 CaT waveforms yielded a high-temporal-resolution CaT curve.

Staining of CD31 and F-actin

For immunofluorescence staining, cells underwent perfusion with 500 μl of cold Dulbecco's phosphate-buffered saline (DPBS), followed by fixation with 500 μl of 4% paraformaldehyde (PFA) and permeabilization with 500 μl of 0.125% Triton X-100 (Nacalai tesque, Kyoto, Japan) at a constant rate of 2,000 μl/h using a peristaltic pump.

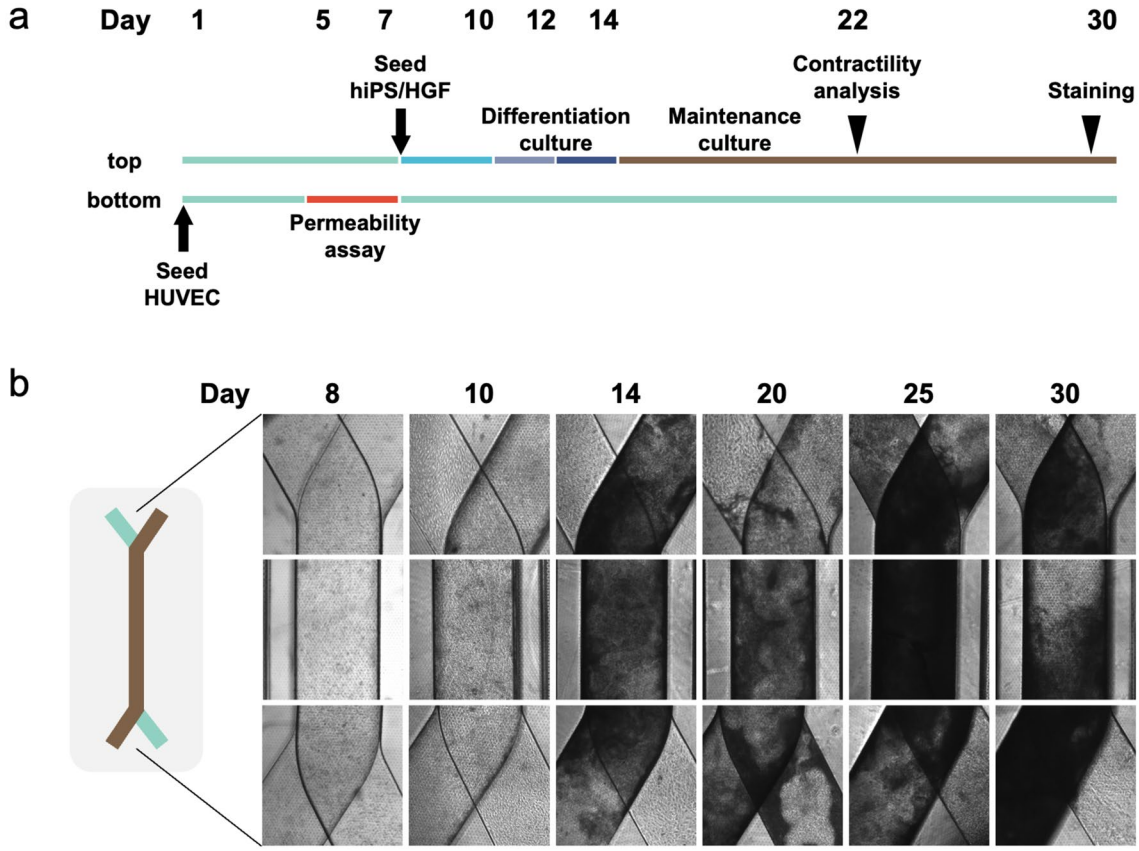

Figure. 8. Timeline for the heart-on-a-chip experiment. (**a**) Endothelial cells are seeded in the bottom channel on Day 1, and a permeability assay is conducted on Days 5–7 to measure permeability. On Day 7, induced pluripotent stem cells and fibroblasts are seeded in the top channel, and the differentiation induction protocol with sequential changes in the culture medium is initiated. Contractility analysis of cardiomyocytes is performed on Day 22, and the experiment concludes on Day 30 with tissue fixation and immunostaining. (**b**) Microscopic images near the inlet (top), middle section (middle), and outlet (bottom) on Days 8, 10, 14, 20, 25, and 30.

Subsequently, 1.5% bovine serum albumin (BSA; Sigma Aldrich, A9418) in DPBS was perfused for blocking for 1 h at a rate of 80 µl/h. Following this, the microfluidic chips were disconnected from the perfusion system. A staining solution consisting of rabbit anti-CD31 primary antibody (Cat. #: ab28364, Abcam, UK) diluted 1:100 in the blocking buffer (1.5% BSA in DPBS) was applied to the bottom channel of the chip. The chip was then refrigerated at 4 °C overnight. After washing the cells with 200 µl/channel DPBS three times, a staining solution containing goat anti-rabbit secondary antibody conjugated with Alexa Fluor 488 (1:1,000 dilution; Cat. #: A-11008, Invitrogen, USA) and ActinRed 555 ReadyProbes Reagent (1:50 dilution; Cat. #: R37112, Invitrogen, USA) was applied to the bottom channel and incubated at room temperature for 1 h. Fluorescence images were captured using a confocal microscope (FLUOVIEW FV1000, OLYMPUS, Japan).

Flow cytometry

For flow cytometry analysis of cardiac tissue, the cells were dissociated into single cells by treating them with 180 µl of 0.25% Trypsin/DMEM (1:2) multiple times for 10 min, and then collected in a 15 ml centrifuge tube. After centrifugation at 300 × g for 5 min, the supernatant was aspirated, and the cells were fixed with a 4% PFA solution at room temperature for 20 min. The cells were then centrifuged again, and the resulting cell pellet was resuspended in 200 µl of ice-cold DPBS. Subsequently, the cells were permeabilized with 0.125% Triton X-100 for 20 min and blocked with 1.5% BSA in PBS at 4 °C for at least 1 h.

After collecting the cells by centrifugation, they were incubated with a 90 µl primary antibody solution containing mouse anti-cTnT primary andibody (1:100; Cat. #: MA5-12960, Invitrogen, USA) and rabbit anti-IRX4 primary antibody (1:100; Cat. #: PA5-97879, Invitrogen, USA) in the blocking solution at 4 °C overnight. Following DPBS washing, the cells were incubated with a secondary antibody solution containing goat anti-mouse secondary antibody conjugated with Alexa Fluor 488 (1:1,000; Cat. #: A32723, Invitrogen, USA) and donkey anti-rabbit secondary antibody conjugated with Alexa Fluor 647 (1:1,000; Cat. #: ab150075, Abcam, UK) in the blocking solution at room temperature for 1 h. Finally, the cells were analyzed using the FACSAria3 cell sorter (BD Biosciences, USA), with 10,000 events recorded for each sample.

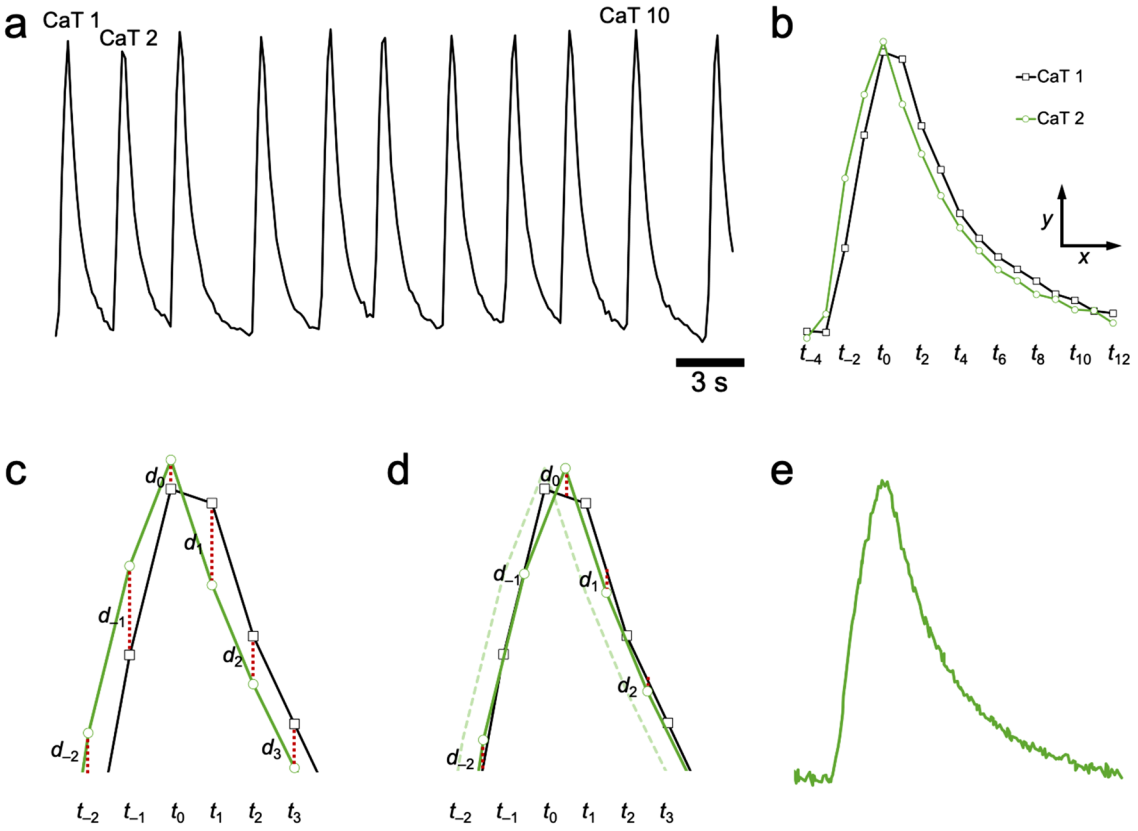

Figure 9. Method to increase temporal resolution of CaT curves. (**a**) Typical CaT trace recorded at an imaging interval of 134 ms. (**b**) Overlay of the first (CaT 1) and the second (CaT 2) CaT curves from the trace in (**a**). t_n indicates the timeframe of imaging. (**c**) Magnified view of (**b**). d_n represents the distance between CaT 1 and CaT 2 curves at each t_n. (**d**) Diagram showing the movement of CaT 2 in the x and y directions to minimize the sum of d_n. (**e**) CaT curves obtained by overlaying 10 curves. In principle, the temporal resolution is increased by 10 times.

Paraffin section staining

To fix the cells, 200 µl of 4% PFA was applied to the top channel of the microfluidic chip and incubated at 4 °C for 12 h. After replacing the PFA solution with DPBS, the microfluidic chip was disassembled, and cardiac tissue was retrieved and embedded in paraffin. Thin sections of 4 µm thickness were prepared, followed by deparaffinization. The sections were then immersed in a tris–EDTA solution with pH 9.0 for antigen retrieval, achieved by microwave heating at 700 W for 20 min.

Subsequently, blocking was conducted at room temperature for 1 h using a 1.5% BSA solution, followed by three DPBS washes. Following this, 100 µl of a staining solution, comprising mouse anti-cTnT primary antibody diluted 1:100 in the blocking buffer, was applied to the tissue section and incubated for 1 h. After three DPBS washes, 100 µl of a staining solution, containing goat anti-mouse secondary antibody conjugated with Alexa Fluor 488 (1:1,000 dilution), ActinRed 555 ReadyProbes Reagent (1:50 dilution), and NucBlue Live ReadyProbes Reagent (1:50 dilution; Cat. #: R37605, Invitrogen, USA), was applied to the tissue section and incubated at room temperature for 1 h. Subsequent to DPBS washing, the tissue section was mounted with ProLong Gold antifade mountant (Cat. #: P10144, Invitrogen, USA) using a coverslip. Fluorescence images were acquired using the FV1000 confocal microscope.

Statistical analysis

Statistical analyses, including sigmoid curve fitting of the dose–response curve for NA and estimation of the EC50 value, were conducted using GraphPad Prism (version 9.5; GraphPad Software, USA). Non-paired Student's t-tests were employed for the assessment of cell directional analysis, CD31 expression levels, myocardial contractility, and myocardial marker expression levels. For the evaluation of vascular endothelial cell layer permeability and CaT analysis in cardiac tissue, one-way analysis of variance with Tukey's post-test was applied. Data are presented as means ± standard error of the mean. A p-value less than 0.05 was considered statistically significant.

Data availability

The flow cytometry data that support the findings of this study are available in FlowRepository at http://flowrepository.org/id/RvFrAmEftJfIAhwSFyqC7kbtpcBAO1KIE0iRWZ3IQjlX7dkc33t4Utmw389Psv3n, reference number FR-FCM-Z7WX.

Received: 9 May 2024; Accepted: 22 July 2024
Published online: 08 August 2024

References

1. Mensah, G. A., Roth, G. A. & Fuster, V. The global burden of cardiovascular diseases and risk factors: 2020 and beyond. *J. Am. Coll. Cardiol.* **74**(20), 2529–2532 (2019).
2. Nerbonne, J. M. Studying cardiac arrhythmias in the mouse—A reasonable model for probing mechanisms?. *Trends Cardiovasc. Med.* **14**(3), 83–93 (2004).
3. Kaese, S. & Verheule, S. Cardiac electrophysiology in mice: A matter of size. *Front. Physiol.* **3**, 345 (2012).
4. Howard, C. M. & Baudino, T. A. Dynamic cell-cell and cell-ECM interactions in the heart. *J. Mol. Cell. Cardiol.* **70**, 19–26 (2014).
5. Zhang, Y. *et al.* Endothelial cells regulate cardiac myocyte reorganisation through beta1-integrin signalling. *Cell. Physiol. Biochem.* **35**(5), 1808–1820 (2015).
6. Chiu, L. L. *et al.* Cardiac tissue engineering: Current state and perspectives. *Front. Biosci. (Landmark Ed.)* **17**(4), 1533–1550 (2012).
7. Radisic, M. & Christman, K. L. Materials science and tissue engineering: Repairing the heart. *Mayo Clin. Proc.* **88**(8), 884–898 (2013).
8. Sharma, A. *et al.* Use of human induced pluripotent stem cell-derived cardiomyocytes to assess drug cardiotoxicity. *Nat. Protoc.* **13**(12), 3018–3041 (2018).
9. Vunjak Novakovic, G., Eschenhagen, T. & Mummery, C. Myocardial tissue engineering: in vitro models. *Cold Spring Harb. Perspect. Med.* **4**(3), a014076 (2014).
10. Cimetta, E., Godier-Furnemont, A. & Vunjak-Novakovic, G. Bioengineering heart tissue for in vitro testing. *Curr. Opin. Biotechnol.* **24**(5), 926–932 (2013).
11. Sakaguchi, K. *et al.* In vitro engineering of vascularized tissue surrogates. *Sci. Rep.* **3**, 1316 (2013).
12. Haraguchi, Y. *et al.* Cell sheet technology for cardiac tissue engineering. *Methods Mol. Biol.* **1181**, 139–155 (2014).
13. Soon, K., Mourad, O. & Nunes, S. S. Engineered human cardiac microtissues: The state-of-the-(he)art. *Stem Cells* **39**(8), 1008–1016 (2021).
14. Zimmermann, W. H., Melnychenko, I. & Eschenhagen, T. Engineered heart tissue for regeneration of diseased hearts. *Biomaterials* **25**(9), 1639–1647 (2004).
15. Bouten, C. V. *et al.* Substrates for cardiovascular tissue engineering. *Adv. Drug Deliv. Rev.* **63**(4–5), 221–241 (2011).
16. Shin, H., Jo, S. & Mikos, A. G. Biomimetic materials for tissue engineering. *Biomaterials* **24**(24), 4353–4364 (2003).
17. Murphy, S. V. & Atala, A. 3D bioprinting of tissues and organs. *Nat. Biotechnol.* **32**(8), 773–785 (2014).
18. Hwang, D. G., Choi, Y. M. & Jang, J. 3D bioprinting-based vascularized tissue models mimicking tissue-specific architecture and pathophysiology for in vitro studies. *Front. Bioeng. Biotechnol.* **9**, 685507 (2021).
19. Zhang, Y. S. *et al.* From cardiac tissue engineering to heart-on-a-chip: Beating challenges. *Biomed. Mater.* **10**(3), 034006 (2015).
20. Mironov, V. *et al.* Biofabrication: A 21st century manufacturing paradigm. *Biofabrication* **1**(2), 022001 (2009).
21. Serpooshan, V. *et al.* The effect of bioengineered acellular collagen patch on cardiac remodeling and ventricular function post myocardial infarction. *Biomaterials* **34**(36), 9048–9055 (2013).
22. Nichol, J. W. *et al.* Cell-laden microengineered gelatin methacrylate hydrogels. *Biomaterials* **31**(21), 5536–5544 (2010).
23. Wu, M. H., Huang, S. B. & Lee, G. B. Microfluidic cell culture systems for drug research. *Lab Chip* **10**(8), 939–956 (2010).
24. Fiddes, L. K. *et al.* A circular cross-section PDMS microfluidics system for replication of cardiovascular flow conditions. *Biomaterials* **31**(13), 3459–3464 (2010).
25. Jastrzebska Jedrych, E. *et al.* Multi-function microsystem for cells migration analysis and evaluation of photodynamic therapy procedure in coculture. *Biomicrofluidics* **6**(4), 44116 (2012).
26. Gwak, S. J. *et al.* The effect of cyclic strain on embryonic stem cell-derived cardiomyocytes. *Biomaterials* **29**(7), 844–856 (2008).
27. Wan, C. R., Chung, S. & Kamm, R. D. Differentiation of embryonic stem cells into cardiomyocytes in a compliant microfluidic system. *Ann. Biomed. Eng.* **39**(6), 1840–1847 (2011).
28. Neal, R. A. *et al.* Three-dimensional elastomeric scaffolds designed with cardiac-mimetic structural and mechanical features. *Tissue Eng. A* **19**(5–6), 793–807 (2013).
29. Chen, M. B. *et al.* A 3D microfluidic platform incorporating methacrylated gelatin hydrogels to study physiological cardiovascular cell-cell interactions. *Lab Chip* **13**(13), 2591–2598 (2013).
30. Ellis, B. W. *et al.* Human iPSC-derived myocardium-on-chip with capillary-like flow for personalized medicine. *Biomicrofluidics* **11**(2), 024105 (2017).
31. Annabi, N. *et al.* Hydrogel-coated microfluidic channels for cardiomyocyte culture. *Lab Chip* **13**(18), 3569–3577 (2013).
32. Pinto, A. R. *et al.* Revisiting cardiac cellular composition. *Circ. Res.* **118**(3), 400–409 (2016).
33. Rook, M. B. *et al.* Differences in gap junction channels between cardiac myocytes, fibroblasts, and heterologous pairs. *Am. J. Physiol.* **263**(5 Pt 1), C959–C977 (1992).
34. Ongstad, E. & Kohl, P. Fibroblast-myocyte coupling in the heart: Potential relevance for therapeutic interventions. *J. Mol. Cell Cardiol.* **91**, 238–246 (2016).
35. Colliva, A. *et al.* Endothelial cell-cardiomyocyte crosstalk in heart development and disease. *J. Physiol.* **598**(14), 2923–2939 (2020).
36. Iwamiya, T. *et al.* Cardiac fibroblast-derived VCAM-1 enhances cardiomyocyte proliferation for fabrication of bioengineered cardiac tissue. *Regen. Ther.* **4**, 92–102 (2016).
37. Matsuda, Y. *et al.* Human gingival fibroblast feeder cells promote maturation of induced pluripotent stem cells into cardiomyocytes. *Biochem. Biophys. Res. Commun.* **503**(3), 1798–1804 (2018).
38. Beauchamp, P. *et al.* 3D Co-culture of hiPSC-derived cardiomyocytes with cardiac fibroblasts improves tissue-like features of cardiac spheroids. *Front. Mol. Biosci.* **7**, 14 (2020).
39. Narmoneva, D. A. *et al.* Endothelial cells promote cardiac myocyte survival and spatial reorganization: Implications for cardiac regeneration. *Circulation* **110**(8), 962–968 (2004).
40. Iyer, R. K. *et al.* Biofabrication enables efficient interrogation and optimization of sequential culture of endothelial cells, fibroblasts and cardiomyocytes for formation of vascular cords in cardiac tissue engineering. *Biofabrication* **4**(3), 035002 (2012).
41. Brodde, O. E., Bruck, H. & Leineweber, K. Cardiac adrenoceptors: Physiological and pathophysiological relevance. *J. Pharmacol. Sci.* **100**(5), 323–337 (2006).
42. Mosqueira, D. *et al.* CRISPR/Cas9 editing in human pluripotent stem cell-cardiomyocytes highlights arrhythmias, hypocontractility, and energy depletion as potential therapeutic targets for hypertrophic cardiomyopathy. *Eur. Heart J.* **39**(43), 3879–3892 (2018).
43. Mesquita, F. C. P. *et al.* R534C mutation in hERG causes a trafficking defect in iPSC-derived cardiomyocytes from patients with type 2 long QT syndrome. *Sci. Rep.* **9**(1), 19203 (2019).
44. Griffith, L. G. & Swartz, M. A. Capturing complex 3D tissue physiology in vitro. *Nat. Rev. Mol. Cell. Biol.* **7**(3), 211–224 (2006).
45. Radisic, M. *et al.* Pre-treatment of synthetic elastomeric scaffolds by cardiac fibroblasts improves engineered heart tissue. *J. Biomed. Mater. Res. A* **86**(3), 713–724 (2008).
46. Yamashiro, Y. & Yanagisawa, H. The molecular mechanism of mechanotransduction in vascular homeostasis and disease. *Clin. Sci. (Lond.)* **134**(17), 2399–2418 (2020).

47. Li, Y. S., Haga, J. H. & Chien, S. Molecular basis of the effects of shear stress on vascular endothelial cells. *J. Biomech.* **38**(10), 1949–1971 (2005).
48. Chistiakov, D. A., Orekhov, A. N. & Bobryshev, Y. V. Effects of shear stress on endothelial cells: Go with the flow. *Acta Physiol. (Oxf.)* **219**(2), 382–408 (2017).
49. Osawa, M. *et al.* Evidence for a role of platelet endothelial cell adhesion molecule-1 in endothelial cell mechanosignal transduction: is it a mechanoresponsive molecule?. *J. Cell Biol.* **158**(4), 773–785 (2002).
50. Zhang, X. H. & Morad, M. Ca(2+) signaling of human pluripotent stem cells-derived cardiomyocytes as compared to adult mammalian cardiomyocytes. *Cell Calcium* **90**, 102244 (2020).
51. Lewis, B. S. *et al.* Effect of the second-generation calcium channel blocker nisoldipine on left ventricular contractility in cardiac failure. *Am. Heart J.* **115**(6), 1238–1244 (1988).
52. Saleem, U. *et al.* Force and calcium transients analysis in human engineered heart tissues reveals positive force-frequency relation at physiological frequency. *Stem Cell Rep.* **14**(2), 312–324 (2020).
53. Sala, L., Gnecchi, M. & Schwartz, P. J. Long QT syndrome modelling with cardiomyocytes derived from human-induced pluripotent stem cells. *Arrhythm. Electrophysiol. Rev.* **8**(2), 105–110 (2019).
54. Veldhuizen, J. *et al.* Cardiac ischemia on-a-chip to investigate cellular and molecular response of myocardial tissue under hypoxia. *Biomaterials* **281**, 121336 (2022).
55. Williams, K. *et al.* A 3-D human model of complex cardiac arrhythmias. *Acta Biomater.* **132**, 149–161 (2021).
56. Le, M. N. T., Takahi, M. & Ohnuma, K. Auto/paracrine factors and early Wnt inhibition promote cardiomyocyte differentiation from human induced pluripotent stem cells at initial low cell density. *Sci. Rep.* **11**(1), 21426 (2021).
57. Rosenblatt-Velin, N. *et al.* FGF-2 controls the differentiation of resident cardiac precursors into functional cardiomyocytes. *J. Clin. Invest.* **115**(7), 1724–1733 (2005).
58. Takahashi, K. *et al.* Live imaging of nitric oxide release in vascular endothelial cells in response to mechanical stimuli on an organ chip. *Eur. Heart J.* **43**, 3027–3027 (2022).
59. Pediaditakis, I. *et al.* A microengineered Brain-Chip to model neuroinflammation in humans. *iScience* **25**(8), 104813 (2022).
60. Liu, Z. Q. Scale space approach to directional analysis of images. *Appl. Opt.* **30**(11), 1369–1373 (1991).

Acknowledgements

We express our gratitude to the Central Research Laboratory at Okayama University Medical School for their valuable assistance in preparing paraffin-embedded tissue sections. This research received support from the Japan Society for the Promotion of Science (JSPS) through Grant-in-Aid for Scientific Research (B) (No. 20H04518) and Grant-in-Aid for Scientific Research (A) (No. 21H04960).

Author contributions

Conceptualization, Y. L., and K. T.; experimental design, Y. L., and K. T.; methodology, R. K., and X. H.; software, M. W., Q. L., and D. L.; analysis, Y. L., R. K., X. H., M. W., Q. L., and D. L.; writing, Y. L.; funding acquisition, K. T., and K. N.

Competing interests

The authors declare no competing interests.

Additional information

Supplementary Information The online version contains supplementary material available at https://doi.org/10.1038/s41598-024-68275-0.

Correspondence and requests for materials should be addressed to K.T.